Formation of a vortex crystal cell assisted by a background vorticity distribution

AUTHOR(S):

Sanpei, A; Kiwamoto, Y; Ito, K; Soga, Y

PHYSICAL REVIEW E **68**, 016404 (2003)

Formation of a vortex crystal cell assisted by a background vorticity distribution

A. Sanpei,[1,*] Y. Kiwamoto,[1,2] K. Ito,[1] and Y. Soga[2]
[1]*Graduate School of Human and Environmental Studies, Kyoto University, Sakyo-ku, Kyoto 606-8501, Japan*
[2]*Faculty of Integrated Human Studies, Kyoto University, Sakyo-ku, Kyoto 606-8501, Japan*
(Received 7 November 2001; revised manuscript received 19 December 2002; published 11 July 2003)

A vortex crystal is a quasistationary, symmetric array of intense vortices (clumps). A low level of background vorticity is experimentally observed to assist three clumps in forming an equilateral triangle starting from initial positions on a linear array. The triangle constitutes a unit cell of a crystal in a many-vortex system. The background vortex curbs the orbital motion of the clumps with unequal strengths to arrest them at the vertices of an equilateral triangle by wrapping them with different sized belts of depleted vorticity (ring holes). We characterize the contributions of a low-level background vorticity distribution on the formation of ordered states of clumps in light of the experimental results and existing theories.

DOI: 10.1103/PhysRevE.68.016404 PACS number(s): 52.27.Jt, 47.32.Cc, 05.65.+b

I. INTRODUCTION

We report an experimental study of a process characterizing one of the most striking features in the relaxation process of two-dimensional (2D) vortical dynamics that leads to an ordered array of intense vortices (vortex crystal). Coherent patches of vorticity are generated from large variety of initial conditions, and often dominate the subsequent evolution of 2D turbulent flows with high Reynold's number [1]. The coherent structures were observed to form spontaneously in numerical studies of freely relaxing 2D turbulence with patches of like sign vorticity [1–4]. A clear experimental demonstration of this process has been given by Fine *et al.* using a strongly magnetized pure electron plasma [5].

The experimental study of 2D vortex dynamics with a magnetized pure electron plasma is based on the equivalence of the macroscopic dynamics of guiding centers to the incompressible fluid. Guiding centers of electrons gyrating in a strong uniform magnetic field $\boldsymbol{B}_0=B_0\hat{z}$ drift with the velocity of $\boldsymbol{v}=\hat{\boldsymbol{z}}\times\boldsymbol{\nabla}\phi(x,y)/B_0$ driven by the electric field $-\boldsymbol{\nabla}\phi(x,y)$. The associated flow is characterized by the vorticity $\zeta\hat{\boldsymbol{z}}=\boldsymbol{\nabla}\times\boldsymbol{v}=\nabla^2\phi/B_0\hat{\boldsymbol{z}}=en/\epsilon_0 B_0\hat{\boldsymbol{z}}$ for a pure electron plasma with particle density $n(x,y)$. Here, ϵ_0 is the dielectric constant in vacuum. In macroscopic scales larger than the gyroradii, this flow is isomorphic to 2D Euler flow in the sense that $\boldsymbol{\nabla}\cdot\boldsymbol{v}=0$, $\zeta(x,y)\propto n(x,y)$, and the stream function is given as $\psi(x,y)=\phi(x,y)/B_0$ [6,7]. The electric properties of the guiding-center particles allow precise control of the initial conditions of $\zeta(x,y)$ and detailed measurements of $\zeta(x,y)$ in its relaxation process. This feature has benefited electron plasma experiments in demonstrating fundamental features of vortex dynamics such as Hamiltonian properties of vortex strings in vacuum [8–10], merging of discrete vortices [11], climbing motion of vortex string (clump) along the slope of the background vortex [12–14], dynamics of vorticity holes in the background vortex [13–15], and the formation of vortex crystals [5,16,17].

The dynamics of mutually interacting point vortices has been the subject of theoretical and simulational studies of 2D turbulence [18–20]. The experiment by Fine *et al.* [5] and a subsequent simulational study by Schecter *et al.* [16] were the first to reveal the important role of the interaction between the strong patches of vorticity (clumps) and the low-level vorticity filling the space around the clumps in the vortical relaxation processes toward the crystal structures. In addition, the background vorticity (BGV) was called for in the statistical model that successfully reproduced the observed crystal arrays of electron vortices [17].

The purpose of this paper is to experimentally examine the contribution of the BGV to the relaxation of the clumps' dynamics toward the formation of a crystal structure. To simplify the problem and quantify the degree of order, we focus on the dynamics of three clumps which are the minimum to form a unit cell in 2D crystal structures. The major difference from previous work is that the shape and level of the initial distribution of the BGV are controlled by preparing the BGV separately before immersion of clumps whose circulations and positions are also controlled. In previous work [11], the clumps were generated by diocotron instability (equivalent to Kelvin-Helmholtz instability) which inevitably deteriorates the reproducibility of the repeated experimental shots coupled with destructive observation of the vorticity distributions made at different times in the relaxation process.

The outline of this paper is as follows: First we examine the time evolution of the triangle pattern of three clumps initially placed either in vacuum or in different levels of the BGV distribution (BGVD). Then quantitative analyses are made in terms of the degree of symmetrization. Finally, we report the observation that even clumps with unequal circulations can form a symmetric cell when surrounded by unevenly depleted zones in the BGVD.

II. EXPERIMENTAL APPARATUS AND METHOD

The experiment is carried out in a Malmberg-type trap as shown in Fig. 1. An axially confining electrostatic potential is maintained in a homogeneous magnetic field of strength $B_0=0.048$ T by grounding the axially aligned 11 conducting cylinders and by negatively biasing the 54-mm-long plug cylinders at both ends. The diameter of the conducting wall

*Email address: n50117@sakura.kudpc.kyoto-u.ac.jp

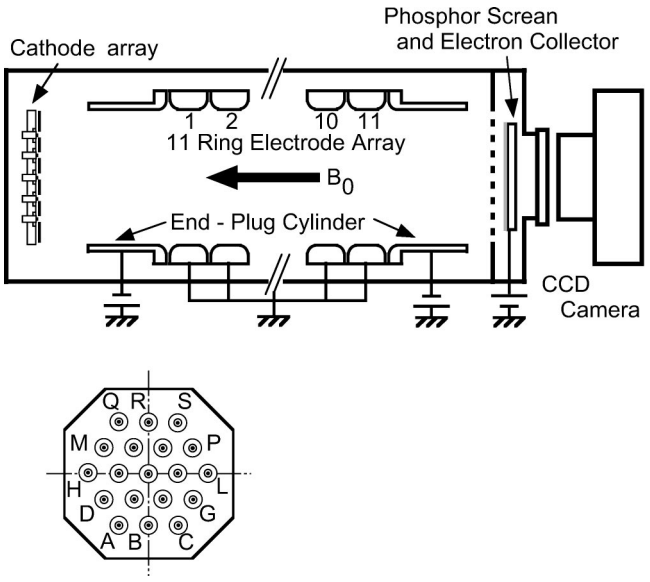

FIG. 1. Schematic configuration of the vortex experiment with pure electron plasma.

is 64 mm. With this vacuum field configuration, the typical axial length of the trapped electron distribution is 235 ± 5 mm.

The electrons are injected from preselected cathode elements, which constitute a cathode array as shown in Fig. 1, into the central region through the temporarily decreased potential barrier at the left end plug. The emission current from each of the selected cathodes is adjusted independently by variable external resistors in order to control the initial vorticity distribution. The BGV with a smooth distribution is generated by mixing and relaxation of hundreds of vortex strings which are repeatedly injected and trapped and then partially ejected leftward. We inject clumps on top of the established BGVD.

Vortex electrons are dumped along the magnetic field lines and collected on the conducting phosphor screen on elimination of the potential barrier at the right end at the required time of observation. The density distribution is measured in terms of the luminosity distribution on the phosphor screen. The phosphor screen is placed at a location where the magnetic field is $0.77B_0$ so that it provides an enlarged image of the distribution projected onto the midplane of the trap. The plasma-facing side of the phosphor screen is coated with 20-nm-thick aluminum so as to prevent deformation of images due to charging up as well as to absolutely determine the total number of collected electrons N. The acceleration voltage of 7.5 kV is applied to the aluminum surface for electrons to penetrate into the phosphor overcoming the stoppering loss of 4.5 keV.

Two-dimensional luminosity distributions on the phosphor plate are measured with a charge-coupled-device camera with 512×512 pixels array and 16 bits of dynamic range. In most cases, we combine 2×2 pixels into 1 pixel to reduce the data size to 256×256 pixels. The distance between the centers of neighboring 2×2 binned pixels corresponds to 146 μm at the midplane. We have confirmed a linear relationship between the line density $n_c(x,y)=\int dz n_c(x,y,z)$ and the luminosity [12,21].

The time evolution of the vorticity distribution is studied by repeating the generation of the initial distribution and destructive diagnostics. The reproducibility of the data reported here is characterized by $\pm 3\%$ dispersion of N for the same physical shots.

III. BGV-ASSISTED FORMATION OF A SYMMETRIC CELL

In Fig. 2, we compare the time evolution of a set of three clumps in vacuum (a) and in a BGVD (b). The clumps are injected at $t=10$ μ sec, and start to move freely on disconnection from the cathode at $t=18$ μs from the initial distribution aligned in a straight line with the same circulation $\Gamma_c=\int\int dxdy\zeta_c(x,y)=eN_c/\epsilon_0 B_0 L=1.64\times10^{-6}N_c$. Here, N_c is the total number of electrons constituting each clump with the length of $L=235\pm5$ mm. The time of observation is indicated at the upper left corner. In vacuum, the clumps continue orbital motion with the period of $\tau_R\approx50$ μs without showing any stationary configuration [20]. The collision with residual neutral atoms acts on the dynamics of the clumps as a viscous effect in the time scale of 1 sec. In the time range of $t>100$ ms, the number of the clumps tends to decrease by collision with residual gas or on hitting the conductor wall after distant excursion.

In the presence of the BGVD as shown in Fig. 2(b), however, the clumps move in a limited region to go into an ordered state. Here the initial BGVD is a continuous distribution with the maximum height of $\zeta_b=\zeta_{c0}/60$, where ζ_{c0} is the height of a clump's vorticity and the ratio of the circulation is $\Gamma_b/\Gamma_c=12.7$. At first, clumps show orbital motion with an averaged period of $\tau_R=25$ μs locally wrapping the background vortex around them ($t=75,150$ μs). Then, the BGVD becomes increasingly fine structured in the differential rotation around the clumps [12]. The maximum level of perturbed BGV is $|\delta\zeta_b/\zeta_b|=|\delta n_b/n_b|=0.49$. The perturbations surrounding the clumps eventually evolve into ring holes [16,17,22,23].

In the later stage, the clumps settle down to form a symmetric triangular array and the fine structures in BGV are smoothed out in our coarse-grained observation ($t=5,10$ ms). In vacuum, such a symmetric configuration can be established only when the three clumps are of equal circulation and placed initially in symmetric locations [9,10,20].

For a quantitative analysis of the formation of the symmetric cell, we introduce a symmetry parameter defined as

$$S=12\sqrt{3}\frac{A}{l^2}. \tag{1}$$

Here A is the area and l is the peripheral length of a triangle that has three clumps at its vertices. S is maximized at 1 when the clumps form an equilateral triangle. We examine the clumps' dynamics in different shapes and levels of the BGVD as described in Fig. 3(a). Initially, the clumps are placed in a straight line at the points indicated by arrows

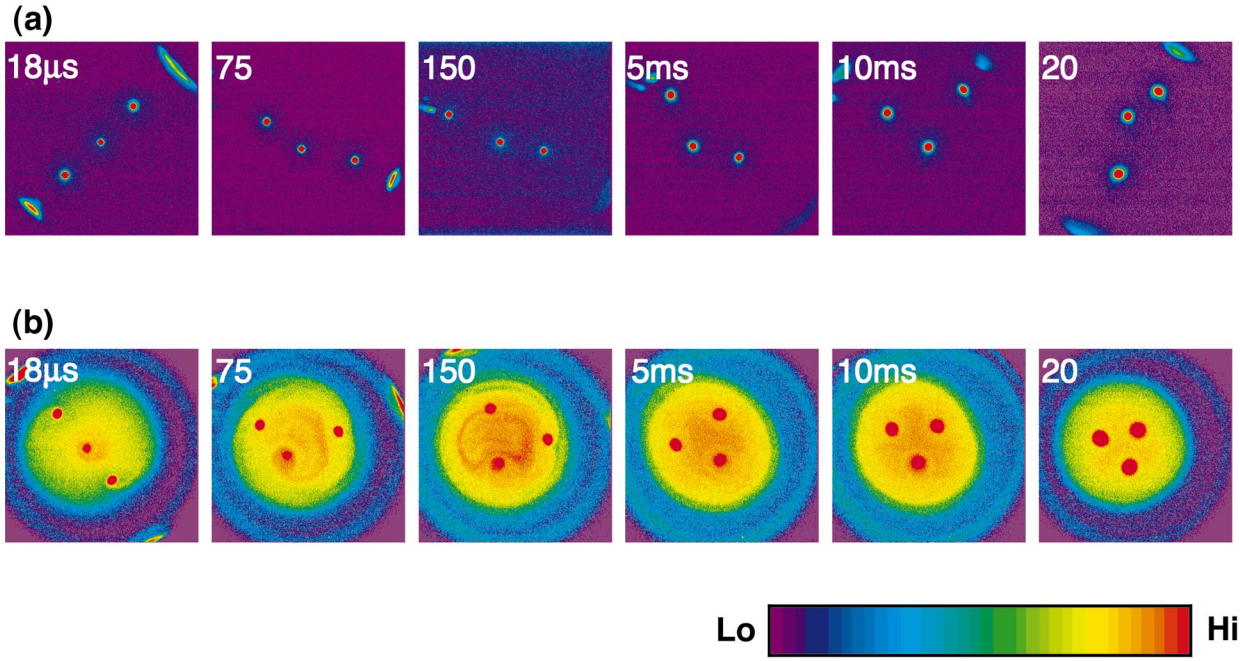

FIG. 2. (Color) Snapshots of the clumps' dynamics in vacuum (a) and in a background vortex with $\Gamma_b \propto N_b/10^7 = 9.4$ (b). These snapshots have the linear luminosity scale with saturation at high level. The clumps with equal strength of $\Gamma_c \propto N_c/10^7 = 0.74$ are placed in line as the initial condition. The panel size is 37.4 mm×37.4 mm.

with equal circulations $\Gamma_c \propto N_c/10^7 = 0.74$. The time evolution as illustrated in Fig. 2(b) is summarized in Fig. 3(b) in terms of $1-S$, representing the degree of deviation from symmetry. The symbols employed in Figs. 3(a) and 3(b) correspond to each other. Two symbols added in Fig. 3(b) represent the cases with $N_b/10^7 = 0.25$ (∇) and 0 ($\times$), i.e., vacuum. The density distribution for ∇ is close to the sensitivity limit of the diagnostics and cannot be determined.

In the initial stage within 100 μs, all symbols for $1-S$ show a common feature of rapid reduction. Here the clumps show kinetic motion weakly modified by the presence of the BGVD. Then comes the next stage of decaying oscillations. The frequency and decay rate of $1-S$ depend on the BGVD. In the vacuum case ($\times$), $1-S$ continues undamped oscillation for $\sim 10^5$ μs until one of the clumps disappears and S becomes undetermined. With the addition of a low-level BGVD ($\triangle$:$N_b/10^7 = 0.52, \zeta_b = \zeta_{c0}/400$), the excursion of the clumps is reduced and the oscillation of $1-S$ damps in the time scale of 1 ms. These features are more evident for higher levels of the BGVD, $N_b/10^7 = 9.4$ (closed $\diamond$), 21.0 ($\square$), 24.8 ($\bigcirc$), but less clear for the case with $N_b/10^7 = 0.25$ (∇). In the third stage of $t \geqslant 10$ ms, $1-S$ further decreases below 10^{-2} without showing strong oscillations. For more than 100 ms in the last stage, we observe stationary configuration in the shape of an equilateral triangle.

For quantitative examination of the relaxation speed of S, we introduce the settling time τ_S as the time after which S remains above 0.9. Figure 4 shows that τ_S decreases as the circulation of the BGVD, $\Gamma_b \propto N_b/10^7$, increases. Almost the same dependence is observed for τ_S vs ζ_b, the height of the BGVD at the initial location of the outermost clump. If τ_S is normalized by the initial turn-over time τ_R, τ_S/τ_R decreases from 120 to 55 as N_b increases. These observations indicate that the BGVD assists the formation of the unit of a vortex crystal.

IV. CONTRIBUTION OF THE BGVD TO COOLING OF CLUMPS' MOTION

The BGVD has been called for as a cooler of randomly moving clumps [5,16]. Fine *et al.* have observed that the average chaotic velocity decreases as $|\delta v| \propto t^{-\alpha}$ with $\alpha = 0.5$–0.6 between $10\tau_R$ and $100\tau_R$ [5]. Schecter *et al.* have evaluated that the exponent α lies between -0.2 and $+0.6$ depending on Γ_b/Γ_{tot} where $\Gamma_{tot} = \Gamma_b + \Gamma_c$ [16].

From Fig. 3(b), we can evaluate the exponent β for the symmetrization by fitting to $1-S \propto t^{-\beta}$. Restricting our analysis to the data at $t \geqslant 200$ μs, i.e., excluding the initial orbital motion, we obtain $\beta = 0.05 \pm 0.21$ for ∇, 0.81 ± 0.28 for $\triangle$, 0.66 ± 0.28 for closed $\diamond$, 0.82 ± 0.22 for $\square$, 0.78 ± 0.21 for $\bigcirc$. If we further limit our analysis for $t > 10^4$ μs, the asymptotic value of β is ~ 1. Figure 5(a) summarizes the cooling exponent β as a function of Γ_b/Γ_{tot}. Starting from zero at $\Gamma_b/\Gamma_{tot} = 0$, β approaches ~ 0.8 and remains there for $0.15 \leqslant \Gamma_b/\Gamma_{tot} < 0.9$. The exponent α quoted from Fig. 10 of Ref. [16] is shown with solid symbols. The observation that β lies around the upper limit of α suggests that β indicates the contribution of the BGVD to the cooling of clumps' motion.

We examine the correspondence between α and β in more detail. We evaluate the root-mean-square value of the velocity fluctuation δv_{rms} as defined by $\delta v_{rms} = (\Sigma_{i=1}^{M} \delta \boldsymbol{v}_i^2/M)^{1/2}$ for M clumps [16]. Here, $\delta \boldsymbol{v}_i = \boldsymbol{v}_i - r_i \bar{\Omega}(t) \hat{\theta}$ is velocity fluctuation about the radial-weighted average rotation $\bar{\Omega}(t) = \Sigma_{i=1}^{M} v_{i,\theta}/\Sigma_{i=1}^{M} r_i$ at the position $\boldsymbol{r}_i$ of

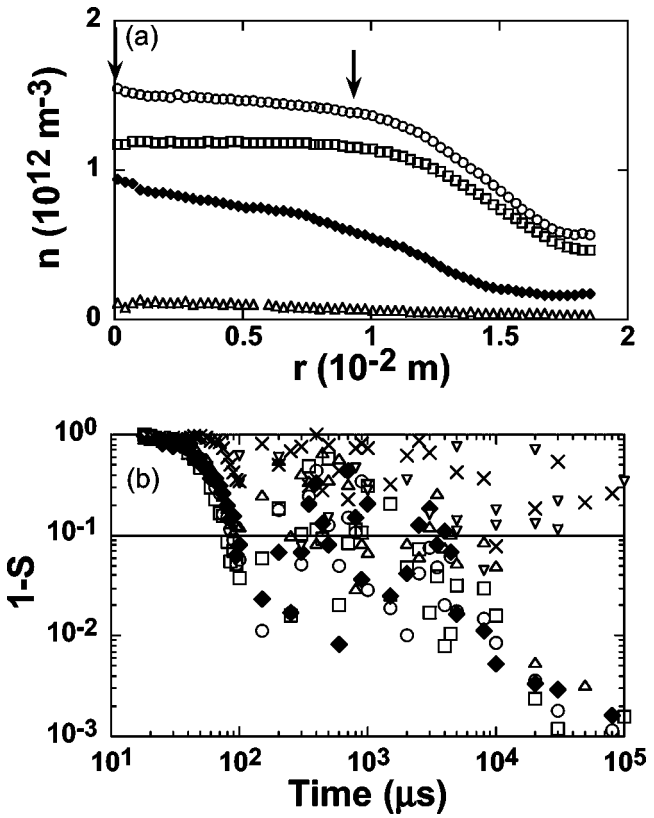

FIG. 3. (a) Radial profiles of the electron density distribution $n_b(x,y)=\epsilon_0 B_0 \zeta_b(x,y)/e$ constituting the background vortices with $N_b/10^7=0.52$ (△), 9.4 (closed ◇), 21.0 (□), and 24.8 (○). The initial radial locations of the clumps are indicated by arrows. (b) Deviation from the symmetry $1-S$ is plotted as a function of time. Each symbol corresponds to the associated profile in Fig. 3(a). The symbols ▽ and × stand for the case with $N_b/10^7=0.25$ and 0, respectively.

the ith clump. The vectors $\boldsymbol{r}_i$ and $\boldsymbol{v}_i$ are evaluated relative to the flow's center of vorticity. The velocity $\boldsymbol{v}_i$ is calculated from the potential distribution $\phi(x,y)$ as determined from the measured density distribution $n(x,y)$. In Fig. 5(b), we directly compare $|\delta v_{rms}|$ with $1-S$ for a typical data representing a similar case to closed ◇ ($N_b/10^7=9.4$). We can observe a correlation given as $|\delta v_{rms}|=(1-S)^{\gamma}$, and obtain a linear relation $\alpha=\gamma\beta$ with $\gamma=0.166\pm0.043$. Applying

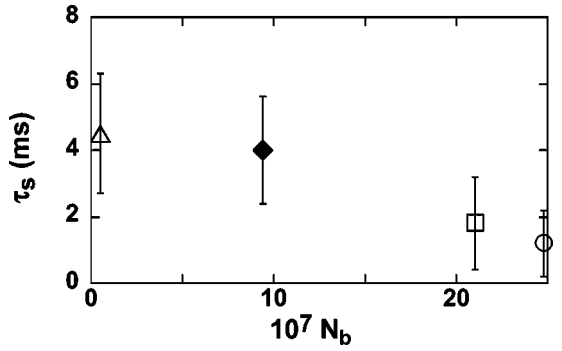

FIG. 4. The settling time τ_S for $S\geqslant 0.9$ is plotted against N_b. Symbols correspond to the profiles in Fig. 3(a).

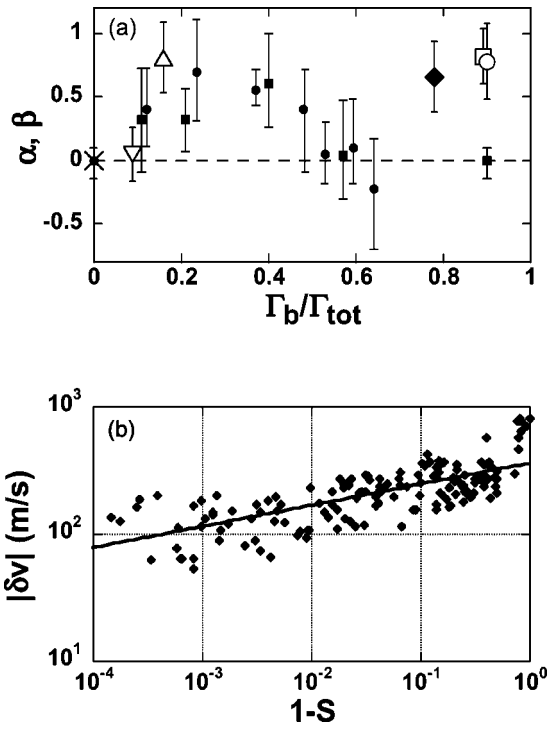

FIG. 5. (a) The exponent β is plotted against Γ_b/Γ_{tot}. Open symbols for β correspond to the profiles in Fig. 3. Small symbols (closed circle and square) represent the α quoted from Fig. 10 of Ref. [16]. (b) $|\delta v_{rms}|$ is plotted against $1-S$ determined from observed data at $t\geqslant 200$ μs. One can draw an empirical relation $|\delta v_{rms}|=(1-S)^{\gamma}$ with $\gamma=0.166\pm0.043$.

this method to other cases, we obtain $\gamma=0.239\pm0.062$ for △, 0.198 ± 0.055 for closed ◇, 0.189 ± 0.041 for □, 0.182 ± 0.059 for ○.

The empirical result $\alpha\sim 0.2\beta$ is useful in the sense that random motion caused by small-scale structures in the electric field can be characterized by the geometrical parameter S. While the accuracy in determining the electric field is severely limited by the spatial resolution of the electron density measurement, say due to coarse graining, the positions of clumps are much easier to determine accurately. Though further examinations are required to assert the role of $1-S$ for $|\delta v_{rms}|$, the usefulness of the parameter S may not be overstated in analyzing the relaxation processes to vortex crystals.

We have assumed that there is no essential difference between Γ_b's in the two analyses. Some discussion should be in order on the difference of the initial distribution of the BGV. In contrast to the previous experiment [5] and simulation [16] where the BGV is generated during the initial instability or through merging between clumps, a smooth distribution of the BGV is imposed in the present experiment. After extensive observations and analyses, we have come to the conclusion that parameters characterizing the initial profile of the BGV are not so influential as the circulation Γ_b. This may be attributed to the observed fact that the smooth distribution of the BGV is quickly scrabbled into rugged distribution by the clumps' motion. However, the wavy distribution of α against Γ_b/Γ_{tot} observed in the previous work

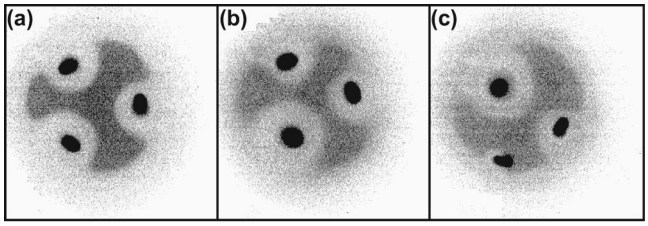

FIG. 6. Quasistationary configurations of three clumps immersed in the background vortex: $(N_{c1},N_{c2},N_{c3},N_b)/10^7=$ (a) (1.1, 1, 0.93, 12); (b) (1.4, 0.84, 0.74, 12); (c) (1.6, 0.93, 0.42, 11). Clumps with unequal circulations form an equilateral triangle only in the presence of the BGVD.

[16] is absent for β, and it may reflect some difference in the origin and history of the BGVD.

V. EQUILIBRIUM STATE OF CLUMPS SUPPORTED BY RING HOLES

An important feature characterizing the structures in the BGVD is a ring hole, a depleted zone of vorticity surrounding a clump. A ring hole is generated when a part of the distribution of an inhomogeneous BGV is advected by a clump [22,23]. Figure 6 shows the vorticity distributions recorded in a quasistationary state at $t \geqslant 5$ ms for different combinations of clumps immersed in the almost identical initial distributions of the BGV. Different sizes of ring holes are clearly observed around the clumps. The BGVD enables a set of extremely unbalanced clumps to form an equilateral triangle with their center of mass keeping the orbital motion.

Modification of the BGVD in the shape of ring holes has been observed in experiments [5] and in a simulation [16]. It was called for in a statistical model [17]. We evaluate the circulation Γ_h of the ring holes by integrating the deficit of the vorticity $\delta\zeta_b(x,y)$ from the smoothly interpolated distribution $\overline{\zeta_b}(x,y)$ of the BGVD, i.e., $\Gamma_h=\int\int dxdy\ \delta\zeta_b(x,y) =\int\int dxdy\ \{\overline{\zeta_b}(x,y)-\zeta_b(x,y)\}$. Here, $\delta\zeta_b(x,y)$ is schematically illustrated by the hatch in the inset of Fig. 7. Figure 7 plots $N_h \propto \Gamma_h$ as a function of $N_c \propto \Gamma_c$ for each clump shown in Fig. 6. It indicates that Γ_h increases with Γ_c for each combination of the clumps and that all the data points lie within a narrow belt demonstrating a good positive correlation between Γ_h and Γ_c. It should be noted, however, that Γ_h remains less than 20% of Γ_c. Therefore, the effective circulations, $\Gamma_{eff}=\Gamma_c-\Gamma_h \propto (N_c-N_h)/10^6$, are (7.9, 7.5, 8.2) for △, (13, 6.1, 6.6) for ○, and (14, 7.3, 6.2) for □. In a statistical model, it is requested for crystallization of vortices that the circulations of the clumps are not fully canceled by the holes in the BGVD [17].

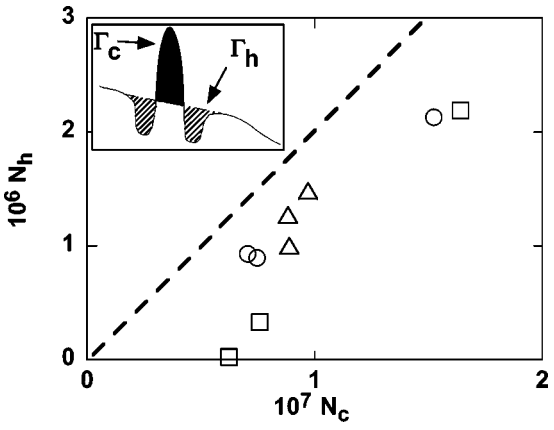

FIG. 7. The circulation Γ_h of ring holes is plotted as a function of the circulation Γ_c of the associated clump. The integrands $\delta\zeta_b(x,y)$ and $\zeta_c(x,y)$ are schematically illustrated in the inset as hatched and dark regions, respectively. The symbols represent different sets of clumps in Fig. 6, △ for (a), ○ for (b), and □ for (c).

The symmetric distribution as observed in Fig. 6(a) is understandable in terms of the force balance among three clumps if their effective circulations Γ_{eff} are equal. We have confirmed experimentally that three clumps with equal circulation Γ_c in the absence of the BGVD are able to maintain the equilateral triangle for more than 100 turns when they were initially placed in the symmetrical position far from the wall. However, there is no clear experimental observation that three clumps with unequal circulation Γ_c can maintain the initial pattern of the equilateral triangle in the vacuum. The role of the BGVD on symmetrization of clumps is discussed in the following section.

VI. DISCUSSION AND CONCLUSION

Aref has predicted that an equilateral configuration can be maintained in the absence of the BGVD if three point vortices with unequal circulations are placed at the vertices of the equilateral triangle [20]. Lansky and O'Neil, on the other hand, have pointed out destabilizing effects of boundary wall unless it is far apart from the clumps even with equal circulations [24]. We extend our discussion in light of these theories.

Our observation indicates that the BGVD plays a decisive role in advecting the clumps from the initial positions aligned in a straight line toward vertices of an equilateral triangle. This process is accompanied by generation of rough structures in the BGVD with length scales larger or comparable with the clumps' radii. As indicated by oscillations of $1-S$, the clumps do not settle down there until the length scales of the BGVD structure decrease further. The observed correlation between $1-S$ and δv indicates that fluctuations in the BGVD cool the clumps' motion and help them settling down at the vertices of the equilateral triangle with $S=1$. Another contribution of the BGVD sets in when the clumps are enclosed by the macroscopically smooth and almost flat BGVD. Observation indicates that equilateral triangle of clumps with unequal circulations is maintained as theoretically predicted by Aref. A difference is that it is realized experimentally only in the presence of the BGVD.

Theoretical analyses on stability have been concentrated on arrays of clumps without the BGVD [24,25]. A well-known prediction is that a conducting wall surrounding the clumps has a destabilizing effect on the array and it has been confirmed in experiments on two-clumps' motion without the BGVD [8]. There is an interesting theoretical finding that a disk-shaped BGVD generates images of clumps at the periphery and behaves as a boundary wall [17]. If this process

is singly dominant, the BGVD may destroy the equilateral triangle configuration contrary to our observation. Ito *et al.* have pointed out experimentally that a BGVD extending beyond the clump tends to shield or at least smear the clump-induced image charge distribution on the wall [21]. If a distinct image of each clump is blurred, the clump-wall interaction is less positionally sensitive, and destabilizing effect of the wall weakens. This process fits more comfortably to our observation than the Jin-Dubin process. The mildly descending profile of the actual BGVD at the periphery may cause the departure from the theoretical model assuming a clear-cut boundary.

In conclusion, we have reported an observation revealing a strong influence of a low-level BGVD on the formation of ordered states of clumps. The BGVD curbs the motion of three clumps to arrest them at the vertices of an equilateral triangle constituting a unit cell of vortex crystal. The settling time to the quasistationary state is shorter for the higher levels of the BGVD. The settling process quantified by the symmetry parameter S is related to the reduction of random velocities δv of the clumps. The clumps generate ring holes (depleted zone of vorticity) around them and tend to partially compensate the imbalance among the circulations. Mixing processes beyond the holes in the BGVD lead to a macroscopically smooth disk-shaped vorticity distribution, and it prepares conditions to support an equilateral triangle array of clumps with unequal circulations, which was predicted by Aref to exist without the BGVD.

ACKNOWLEDGMENTS

This work was supported by a Grant-in-Aid from the Ministry of Education, Culture, Sports, Science and Technology and by the collaborative research program of the National Institute for Fusion Science. We appreciate Professor Y. Fukumoto of Kyushu University pointing out Aref's equilibrium solution for three unequal point vortices.

[1] J.C. MacWilliams, J. Fluid Mech. **146**, 21 (1984).
[2] R. Benzi, S. Patarnello, and P. Santangelo, J. Phys. A **21**, 1221 (1988).
[3] G.F. Carnevale, J.C. McWilliams, Y. Pomeau, J.B. Weiss, and W.R. Young, Phys. Rev. Lett. **66**, 2735 (1991).
[4] T. Watanabe, T. Iwayama, and H. Fujisaka, Phys. Rev. E **57**, 1636 (1998).
[5] K.S. Fine, A.C. Cass, W.G. Flynn, and C.F. Driscoll, Phys. Rev. Lett. **75**, 3277 (1995).
[6] R.H. Levy, Phys. Fluids **11**, 920 (1968).
[7] R.J. Briggs, J.D. Daugherty, and R.H. Levy, Phys. Fluids **13**, 421 (1970).
[8] T.B. Mitchell, C.F. Driscoll, and K.S. Fine, Phys. Rev. Lett. **71**, 1371 (1993).
[9] Y. Kiwamoto, A. Mohri, K. Ito, A. Sanpei, and T. Yuyama, in *Non-Neutral Plasma Physics* III, edited by John J. Bollinger, Ross L. Spencer, and Ronald C. Davidson, AIP Conf. Proc. No. 498 (AIP, Melville, NY, 1999), pp. 99–105.
[10] Y. Kiwamoto, K. Ito, A. Sanpei, A. Mohri, T. Yuyama, and T. Michishita, J. Phys. Soc. Jpn. **68**, 3766 (1999).
[11] K.S. Fine, C.F. Driscoll, J.H. Malmberg, and T.B. Mitchell, Phys. Rev. Lett. **67**, 588 (1991).
[12] Y. Kiwamoto, K. Ito, A. Sanpei, and A. Mohri, Phys. Rev. Lett. **85**, 3173 (2000).
[13] D.A. Schecter and D.H.E. Dubin, Phys. Rev. Lett. **83**, 2191 (1999).
[14] D.A. Schecter and D.H.E. Dubin, Phys. Fluids **13**, 1704 (2001).
[15] X.-P. Huang, K.S. Fine, and C.F. Driscoll, Phys. Rev. Lett. **74**, 4424 (1995).
[16] D.A. Schecter, D.H.E. Dubin, K.S. Fine, and C.F. Driscoll, Phys. Fluids **11**, 905 (1999).
[17] D.Z. Jin and D.H.E. Dubin, Phys. Rev. Lett. **80**, 4434 (1998).
[18] L. Onsager, Nuovo Cimento **6**, 276 (1949).
[19] G. Joyce and D. Montgomery, J. Plasma Phys. **10**, 107 (1973).
[20] H. Aref, Phys. Fluids **22**, 393 (1979).
[21] K. Ito, Y. Kiwamoto, and A. Sanpei, Jpn. J. Appl. Phys., Part 1 **40**, 2558 (2001).
[22] A. Sanpei, Y. Kiwamoto, and K. Ito, J. Phys. Soc. Jpn. **70**, 2813 (2001).
[23] D. Durkin and J. Fajans, Phys. Rev. Lett. **85**, 4052 (2000).
[24] I.M. Lansky and T.M. O'Neil, Phys. Rev. E **55**, 7010 (1997).
[25] T.H. Havelock, Philos. Mag. **11**, 617 (1931).